IEEE Photonics Journal
An IEEE Photonics Society Publication

Open Access

Comparison of Two Two-Photon Dressed Rules in Multi-Wave Mixing

Volume 6, Number 1, February 2014

Jia Sun
Peiying Li
Gaoping Huang
Yunzhe Zhang
Dan Zhang
Hao Tian
Heqing Huang
Yanpeng Zhang

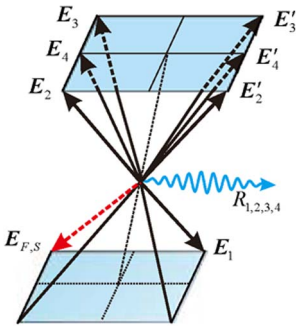

DOI: 10.1109/JPHOT.2014.2300498
1943-0655

IEEE photonics SOCIETY

IEEE

Comparison of Two Two-Photon Dressed Rules in Multi-Wave Mixing

Jia Sun, Peiying Li, Gaoping Huang, Yunzhe Zhang, Dan Zhang, Hao Tian, Heqing Huang, and Yanpeng Zhang

Key Laboratory for Physical Electronics and Devices of the Ministry of Education & Shaanxi Key Lab of Information Photonic Technique, Xi'an Jiaotong University, Xi'an 710049, China

DOI: 10.1109/JPHOT.2014.2300498

Manuscript received November 4, 2013; accepted January 7, 2014. Date of publication January 16, 2014; date of current version January 27, 2014. This work was supported in part by the 973 Program under Grant 2012CB921804; by the NSFC under Grants 61308015, 61078002, 61078020, 11104214, 61108017, 11104216, and 61205112; by the RFDP under Grants 20110201110006, 20110201120005, and 20100201120031; by the FRFCU under Grants 2011jdhz07, xjj2011083, xjj2011084, 2012jdhz05, xjj2012080, and xjj2013089; and by the CPSF under Grant 2012M521773. Corresponding author: Y. Zhang (e-mail: ypzhang@mail.xjtu.edu.cn).

Abstract: For the first time, we report a novel two-photon dressed rule in a five-level ^{85}Rb atomic system. In comparison with a traditional two-photon dressed rule where the signals move with probe field frequency detuning changing, the novel one indicates that the signals do not move with coupling field frequency detuning changing. The finding is verified by the experimentally detected transmitted probe, multi-wave mixing, and fluorescence signals. We also find that the fluorescence signals show Autler–Townes splitting, which are observed experimentally and explained theoretically. By scanning one coupling field frequency detuning, variation of the dressing strength of another coupling field is revealed. Finally, we demonstrate that the alternation can be phase controlled if one of the incident beams deviates an angle (i.e., change from a normal state to an abnormal state).

Index Terms: Aulter–Townes splitting, multi-wave mixing, electromagnetically induced transparency.

1. Introduction

Multi-wave mixing (MWM) processes enhanced by atomic coherence have been experimentally studied in several atomic systems [1], [2]. One of the vital factors to obtain such enhanced nonlinear optical processes is the drastically reduced absorption of the generated optical field due to electromagnetically induced transparency (EIT) [3], [4], which has been reported in photon controlling and information storage [5], [6], quantum communications [7], nonlinear optics and wave-mixing process [8], [9]. In last decade, we demonstrated that the coexistence of six-wave mixing (SWM) and four-wave mixing (FWM) processes; we found the SWM can be comparable in amplitude with the FWM by manipulating the atomic coherence and multi-photon interferences between different energy levels [1], [10], [11]. Such coherent control technique allows us to control the transition probability in atoms [12], photoelectron angular distribution [13], and various chemical reactions.

Besides, as an important phenomenon related with EIT, Autler–Townes (AT) splitting was first studied on a radio-frequency transition [14] more than a half century ago. Later, AT splitting effect was observed in lithium molecules [15] and semiconductor material [16]. Recently, this effect in

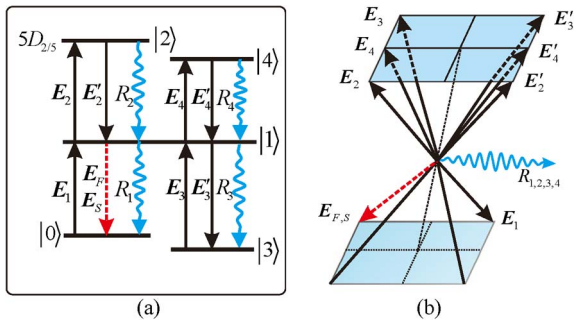

Fig. 1. (a) K-type four-level atomic system of ^{85}Rb. (b) Spatial geometry of relevant beams.

FWM and SWM processes has been experimentally demonstrated by scanning the probe field in EIT windows [17], [18]. Moreover, the AT splitting effect in fluorescence due to spontaneous emission was also observed under EIT conditions [19], [20].

In this paper, we change the probe field frequency detuning and coupling field frequency detuning to investigate and compare the two two-photon dressed rules, which gives rise to the moved or fixed EIT of probe transmission signal (PTS), enhancement/suppression of MWM and AT splitting of the accompany fluorescence signals. We also reveal that the dressed strength of one coupling beam is changeable with interval between probe field and dressed energy levels changed, which is induced by changing the detuning of the other coupling beam. By changing one coupling field frequency detuning and scanning another coupling field frequency detuning, we also investigate the phase control effects on the PTS, MWM and fluorescence signals.

2. Experimental Scheme and Basic Theory

2.1. Experimental Scheme

The experiment is performed in ^{85}Rb vapors, and the involving five energy levels $5S_{1/2}(F=3)(|0\rangle)$, $5P_{3/2}(\mathrm{F}=4)(|1\rangle)$, $5D_{5/2}(|2\rangle)$, $5S_{1/2}(F=2)(|3\rangle)$, and $5D_{3/2}(|4\rangle)$ can form a K-type level system as shown in Fig. 1(a). A weak laser beam $\boldsymbol{E}_1$ (with wavelength 780.245 nm, frequency ω_1, wave vector $\mathbf{k}_1$, power P_1, Rabi frequency G_1, frequency detuning Δ_1, and horizontally polarized) probes the lower transition $|0\rangle \rightarrow |1\rangle$. Here, $\Delta_i = \Omega_i - \omega_i$ with Ω_i being the resonant frequency of transition driven by E_i, and $G_i = \mu_i E_i/\hbar$ with transition dipole moment μ_i. Two strong pumping beams $\boldsymbol{E}_3$ & $\boldsymbol{E}_3'$ (780.235 nm, ω_3, $\mathbf{k}_3(\mathbf{k}_3')$, $G_3(G_3')$, Δ_3, and vertically polarized) drive $|3\rangle \rightarrow |1\rangle$, and two pairs of strong coupling beams $\boldsymbol{E}_2$ & $\boldsymbol{E}_2'$ (775.978 nm, ω_2, $\mathbf{k}_2(\mathbf{k}_2')$, $P_2(P_2')$, $G_2(G_2')$, Δ_2, and vertically polarized) and $\boldsymbol{E}_4$ & $\boldsymbol{E}_4'$ (776.157 nm, ω_4, $\mathbf{k}_4(\mathbf{k}_4')$, $G_4(_{G_4}')$, Δ_4, and vertically polarized) connect $|1\rangle \rightarrow |2\rangle$ and $|1\rangle \rightarrow |4\rangle$, respectively. The laser beams are aligned spatially as shown in Fig. 1(b), where the pumping and coupling beams propagate through ^{85}Rb vapor cell (with a temperature of 60 °C) in the same direction with a small angle $(\sim 0.3^\circ)$ while $\boldsymbol{E}_1$ counter-propagates with $\boldsymbol{E}_2$.

There exist two ladder-type EIT windows in this system, i.e., the ladder-type subsystems $|0\rangle \rightarrow |1\rangle \rightarrow |2\rangle$ and $|0\rangle \rightarrow |1\rangle \rightarrow |4\rangle$, which satisfy the two-photon Doppler-free conditions. When all the seven laser beams mentioned above are on, three FWM processes $\boldsymbol{E}_{F2}$ (satisfying the phase-matching condition $\mathbf{k}_{F2} = \mathbf{k}_1 + \mathbf{k}_2 - \mathbf{k}_2'$), $\boldsymbol{E}_{F4}(\mathbf{k}_{F4} = \mathbf{k}_1 + \mathbf{k}_4 - \mathbf{k}_4')$, and $\boldsymbol{E}_{F3}(\mathbf{k}_{F3} = \mathbf{k}_1 + \mathbf{k}_3 - \mathbf{k}_3')$, as well as four SWM processes $\boldsymbol{E}_{S2}(\mathbf{k}_{S2} = \mathbf{k}_1 - \mathbf{k}_3' + \mathbf{k}_3 + \mathbf{k}_2 - \mathbf{k}_2)$, $\boldsymbol{E}_{S2}'(\mathbf{k}_{S2}' = \mathbf{k}_1 - \mathbf{k}_3' + \mathbf{k}_3 + \mathbf{k}_2' - \mathbf{k}_2')$, $\boldsymbol{E}_{S4}(\mathbf{k}_{S4} = \mathbf{k}_1 - \mathbf{k}_3' + \mathbf{k}_3 + \mathbf{k}_4 - \mathbf{k}_4)$, and $\boldsymbol{E}_{S4}'(\mathbf{k}_{S4}' = \mathbf{k}_1 - \mathbf{k}_3' + \mathbf{k}_3 + \mathbf{k}_4' - \mathbf{k}_4')$ can be generated simultaneously. The propagation direction of all the generated signals with horizontal polarization propagates along the same direction with a bit deviation from probe beam, as shown in Fig. 1(b). The wave-mixing signals are detected by an avalanche photodiode detector, while the PTS is detected by a silicon photodiode. Besides, as shown in Fig. 1(a), four fluorescence signals (R_{1-4}) due to spontaneous emission are also detected simultaneously by another photodiode,

where the odd pair R_1 and R_3 with same wavelength of 780 nm are both caused by the decay from $|1\rangle$; while the even pair R_2 and R_4 with same wavelength of 776 nm are caused by the decays from $|2\rangle$ and $|4\rangle$, respectively.

2.2. Basic Theory

In general, we can solve the coupled density-matrix equations to obtain $\rho_{10}^{(1)}$, $\rho_{10}^{(3)}$, and $\rho_{10}^{(5)}$ for PTS, FWM and SWM processes, respectively, and $\rho_{11R_1}^{(2)}$, $\rho_{11R_3}^{(2)}$, $\rho_{22}^{(4)}$, $\rho_{44}^{(4)}$ for fluorescence signals.

For PTS, the perturbation chain $\rho_{00}^{(0)} \xrightarrow{G_1} \rho_{10}^{(1)}$ leads to

$$\rho_{10}^{(1)} = iG_1 / \left[\left(d_1 + |G_2|^2 / d_2 + |G_4|^2 / d_6 \right) \right]$$

where $d_1 = \Gamma_{10} + i\Delta_1$, $d_2 = \Gamma_{20} + i(\Delta_1 + \Delta_2)$, $d_6 = d_4 + |G_1|^2/(\Gamma_{41} + i\Delta_4)$, $d_4 = \Gamma_{40} + i(\Delta_1 + \Delta_4)$, and Γ_{ij} is transverse relaxation rate between $|i\rangle$ and $|j\rangle$. Here, the dressed effects of $\boldsymbol{E}_2$ and $\boldsymbol{E}_4$ are considered due to the high intensities of the fields. As to FWM signal $\boldsymbol{E}_{F2}$, the perturbation chain $\rho_{00}^{(0)} \xrightarrow{G_1} \rho_{10}^{(1)} \xrightarrow{G_2} \rho_{20}^{(2)} \xrightarrow{(G_2')^*} \rho_{10}^{(3)}$ leads to

$$\rho_{10F2}^{(3)} = -iG_1 G_2 (G_2')^* / \left[\left(d_1 + |G_2|^2 / d_2 + |G_1|^2 / d_5 + |G_4|^2 / d_6 \right)^2 d_2 \right]$$

where $d_5 = \Gamma_{11} + |G_4|^2/(\Gamma_{41} + i\Delta_4)$. For $\boldsymbol{E}_{F4}$, the perturbation chain $\rho_{00}^{(0)} \xrightarrow{G_1} \rho_{10}^{(1)} \xrightarrow{G_4} \rho_{40}^{(2)} \xrightarrow{(G_4')^*} \rho_{10}^{(3)}$ gives

$$\rho_{10F4}^{(3)} = -iG_1 G_4 (G_4')^* / \left[\left(d_1 + |G_2|^2 / d_2 + |G_1|^2 / d_5 + |G_4|^2 / d_6 \right)^2 d_4 \right].$$

While for $\boldsymbol{E}_{F3}$, we obtain

$$\rho_{10F3}^{(3)} = -iG_1 G_3 (G_3')^* / \left[\left(d_1 + |G_2|^2 / d_2 + |G_1|^2 / d_5 + |G_4|^2 / d_6 \right)^2 d_3 \right]$$

through the perturbation chain $\rho_{00}^{(0)} \xrightarrow{G_1} \rho_{10}^{(1)} \xrightarrow{(G_3')^*} \rho_{30}^{(2)} \xrightarrow{G_3} \rho_{10}^{(3)}$, where $d_3 = \Gamma_{30} + i(\Delta_1 - \Delta_3)$.

For SWM processes, $\rho_{10}^{(5)}$ could be obtained via following perturbation chains:

$$\rho_{00}^{(0)} \xrightarrow{G_1} \rho_{10}^{(1)} \xrightarrow{G_2} \rho_{20}^{(2)} \xrightarrow{(G_2)^*} \rho_{10}^{(3)} \xrightarrow{(G_3')^*} \rho_{30}^{(4)} \xrightarrow{G_3} \rho_{10S2}^{(5)} \text{ for } \boldsymbol{E}_{S2},$$

$$\rho_{00}^{(0)} \xrightarrow{G_1} \rho_{10}^{(1)} \xrightarrow{G_2'} \rho_{20}^{(2)} \xrightarrow{(G_2')^*} \rho_{10}^{(3)} \xrightarrow{(G_3')^*} \rho_{30}^{(4)} \xrightarrow{G_3} \rho_{10S2}^{\prime(5)} \text{ for } \boldsymbol{E}'_{S2},$$

$$\rho_{00}^{(0)} \xrightarrow{G_1} \rho_{10}^{(1)} \xrightarrow{G_4} \rho_{40}^{(2)} \xrightarrow{(G_4)^*} \rho_{10}^{(3)} \xrightarrow{G_3} \rho_{30}^{(4)} \xrightarrow{(G_3')^*} \rho_{10S4}^{(5)} \text{ for } \boldsymbol{E}_{S4}, \text{and}$$

$$\rho_{00}^{(0)} \xrightarrow{G_1} \rho_{10}^{(1)} \xrightarrow{G_4'} \rho_{40}^{(2)} \xrightarrow{(G_4')^*} \rho_{10}^{(3)} \xrightarrow{G_3} \rho_{30}^{(4)} \xrightarrow{(G_3')^*} \rho_{10S4}^{\prime(5)} \text{ for } \boldsymbol{E}'_{S4}.$$

The corresponding density-matrix elements are

$$\rho_{10S2}^{(5)} = iG_1 |G_2|^2 G_3 (G_3')^* / \left[\left(d_1 + |G_1|^2 / d_5 + |G_2|^2 / d_2 + |G_4|^2 / d_6 \right)^3 d_3 \left(d_2 + |G_1|^2 / d_7 \right) \right]$$

$$\rho_{10S2}^{\prime(5)} = iG_1 |G_2'|^2 G_3 (G_3')^* / \left[\left(d_1 + |G_1|^2 / d_5 + |G_2|^2 / d_2 + |G_4|^2 / d_6 \right)^3 d_3 \left(d_2 + |G_1|^2 / d_7 \right) \right]$$

$$\rho_{10S4}^{(5)} = iG_1 |G_4|^2 G_3 (G_3')^* / \left[\left(d_1 + |G_1|^2 / d_8 + |G_2|^2 / d_2 + |G_4|^2 / d_6 \right)^3 d_3 \left(d_4 + |G_1|^2 / d_9 \right) \right]$$

$$\rho_{10S4}^{\prime(5)} = iG_1 |G_4'|^2 G_3 (G_3')^* / \left[\left(d_1 + |G_1|^2 / d_8 + |G_2|^2 / d_2 + |G_4|^2 / d_6 \right)^3 d_3 \left(d_4 + |G_1|^2 / d_9 \right) \right]$$

where $d_7 = \Gamma_{21} + i\Delta_2 + |G_3|^2/[\Gamma_{23} + i(\Delta_2 + \Delta_3)]$, $d_8 = \Gamma_{11} + |G_2|^2/(\Gamma_{21} + i\Delta_2)$, and $d_9 = \Gamma_{41} + i\Delta_4 + |G_3|^2/[\Gamma_{43} + i(\Delta_4 + \Delta_3)]$.

For fluorescence signals, the density-matrix elements could be obtained via the perturbation chains

$$\rho_{00}^{(0)} \xrightarrow{G_1} \rho_{10}^{(1)} \xrightarrow{(G_1)^*} \rho_{11}^{(2)} \text{ and } \rho_{00}^{(0)} \xrightarrow{(G_1)^*} \rho_{01}^{(1)} \xrightarrow{G_1} \rho_{11}^{(2)} \text{ for } R_1,$$

$$\rho_{33}^{(0)} \xrightarrow{G_3} \rho_{13}^{(1)} \xrightarrow{(G_3)^*} \rho_{11}^{(2)} \text{ and } \rho_{33}^{(0)} \xrightarrow{(G_3)^*} \rho_{31}^{(1)} \xrightarrow{G_3} \rho_{11}^{(2)} \text{ for } R_3,$$

$$\rho_{00}^{(0)} \xrightarrow{G_1} \rho_{10}^{(1)} \xrightarrow{G_2} \rho_{20}^{(2)} \xrightarrow{(G_1)^*} \rho_{21}^{(3)} \xrightarrow{(G_2)^*} \rho_{22}^{(4)} \text{ and}$$

$$\rho_{00}^{(0)} \xrightarrow{(G_1)^*} \rho_{01}^{(1)} \xrightarrow{(G_2)^*} \rho_{02}^{(2)} \xrightarrow{G_1} \rho_{12}^{(3)} \xrightarrow{G_2} \rho_{22}^{(4)} \text{ for } R_2, \text{and}$$

$$\rho_{00}^{(0)} \xrightarrow{G_1} \rho_{10}^{(1)} \xrightarrow{G_4} \rho_{40}^{(2)} \xrightarrow{(G_1)^*} \rho_{41}^{(3)} \xrightarrow{(G_4)^*} \rho_{44}^{(4)} \text{ and}$$

$$\rho_{00}^{(0)} \xrightarrow{(G_1)^*} \rho_{01}^{(1)} \xrightarrow{(G_4)^*} \rho_{04}^{(2)} \xrightarrow{G_1} \rho_{14}^{(3)} \xrightarrow{G_4} \rho_{44}^{(4)} \text{ for } R_4.$$

The corresponding expressions are

$$\rho_{11R_1}^{(2)} = |G_1|^2/\left[\Gamma_{11}\left(d_1 + |G_2|^2/d_2 + |G_4|^2/d_4\right)\right] + h.c.,$$

$$\rho_{11R_3}^{(2)} = |G_3|^2/[\Gamma_{11}(\Gamma_{13} + i\Delta_3)] + h.c.,$$

$$\rho_{22}^{(4)} = |G_1|^2|G_2|^2/\left[\Gamma_{22}d_1d_{10}\left(d_2 + |G_2|^2/d_1\right)\right] + h.c.,$$

$$\rho_{44}^{(4)} = |G_1|^2|G_4|^2/\left[\Gamma_{44}d_1d_{11}\left(d_4 + |G_4|^2/d_1\right)\right] + h.c.$$

where $d_{10} = \Gamma_{21} + i\Delta_2$ and $d_{11} = \Gamma_{41} + i\Delta_4$.

2.3. Judgement for the Dressed Strength

In Ref. [21], when Δ_1 is changed and Δ_4 is scanned, the dressed strength of $\boldsymbol{E}_4$ is decided by the value of Δ_1, and the FWM signal can switch between enhancement and suppression. In other words, the dressed strength of $\boldsymbol{E}_4$ is fixed once Δ_1 is set at a specific value. However, when Δ_2 is changed and Δ_4 is scanned, the dressed strength of $\boldsymbol{E}_4$ could change even at specific Δ_1. The strength is, in fact, determined by the minimum interval between $\boldsymbol{E}_1$ and the dressed energy levels $|\pm\rangle$ caused by $\boldsymbol{E}_2$ and $\boldsymbol{E}_2'$. This interval can be obtained via the Hamiltonian method. The Hamiltonian for the process that the strong fields $\boldsymbol{E}_2$ & $\boldsymbol{E}_2'$ split the state $|1\rangle$ is written as

$$H = -\hbar\begin{pmatrix} 0 & G_2 \\ G_2^* & \Delta_2 \end{pmatrix}. \tag{1}$$

The eigenstates of the Hamiltonian are $|\pm\rangle$ and the eigenvalues $\lambda_\pm$ are

$$\lambda_+ = \left[\Delta_2 + \left(\Delta_2^2 + 4|G_2|^2\right)^{1/2}\right]/2 \tag{2a}$$

$$\lambda = \left[\Delta_2 - \left(\Delta_2^2 + 4|G_2|^2\right)^{1/2}\right]/2. \tag{2b}$$

The dressed states are movable with different values of Δ_2 and G_2. The minimum interval between the field $\boldsymbol{E}_1$ and the dressed energy levels $|\pm\rangle$ is given as

$$Interval = \min\{|\Delta_1 - \lambda_+|, |\Delta_1 - \lambda|\}. \tag{3}$$

Since the field $\boldsymbol{E}_4$ imposes its dressed effect mainly on the region $\Delta_1 + \Delta_4 = 0$ (two-photon condition), its dressed strength is inverse proportional to the value of the *Interval*. Take the case

$\Delta_1 = 0$ for an example, changing $|\Delta_2|$ from zero to some major value will lead to the *Interval* change from large to small, and this will make the dressed strength of $\boldsymbol{E}_4$ alter from weak to strong.

3. Experimental Results and Discussions

For simplicity, we start from the FWM process $\boldsymbol{E}_{F2}$ with $\boldsymbol{E}_3$ & $\boldsymbol{E}_4'$ & $\boldsymbol{E}_4'$ blocked. Based on Δ_4 being scanned with different Δ_1 and Δ_2, the spectra of PTS, FWM and fluorescence signals are measured as shown in Fig. 2. We arrange the curves horizontally to reveal the total profiles of their baselines [Fig. 2(a) and (c)] and vertically to display their locations and details [Fig. 2(b) and (d)]. First, the upper curves in Fig. 2(a1) and (c1) show the PTS at discrete Δ_1 and Δ_2, which is composed by three major parts: baseline (horizontal background), profile (dashed line), and EIT separation embed on the baseline. The baseline height of each curve represents the transmitted intensity of $\boldsymbol{E}_1$ without the dressing effect of $\boldsymbol{E}_4$. The profile reveals an EIT window at $\Delta_1 = -\Delta_2 = 0$ caused by $\boldsymbol{E}_2$, i.e., the term $|G_2|^2/d_2$ in $\rho_{10}^{(1)}$. The EIT separation (twin peaks above the baseline) is mainly caused by the combined nested-cascade dressing effects of $\boldsymbol{E}_1$ and $\boldsymbol{E}_4$ (presented by $|G_4|^2/d_6$ in $\rho_{10}^{(1)}$). The strength of EIT separation is weak near the region $\Delta_1 = 0$ or $\Delta_2 = 0$, corresponding to the weak dressed strength of $\boldsymbol{E}_4$ with large value of *Interval*. Second, the middle curves show the FWM signal in Fig. 2(a2) and (c2), including three parts also, i.e., baseline, profile and suppression separation embedded on the baseline. Similarly, every baseline height represents the intensity of $\boldsymbol{E}_{F2}$ without the dressing effect of $\boldsymbol{E}_4$. The profile (dashed line) reaches its maximum near $\Delta_1 = -\Delta_2 = 0$. The suppression separation (twin dips below the baseline) appears once Δ_4 is scanned. So, the suppression separation is corresponding to the EIT separation and mainly determined by $|G_4|^2/d_6$ in $\rho_{10F2}^{(3)}$. Third, the lower curves in Fig. 2(a3) and (c3) show the fluorescence signals, where the profile (dashed line) reflects the background intensity of $R_1 + R_2$. The suppression dip that appears at large value of $|\Delta_1|$ or $|\Delta_2|$ becomes shallow gradually and becomes invisible at $|\Delta_1| = 0$ or $|\Delta_2| = 0$ eventually, which corresponds to the weakening process of EIT. Two peaks (belonging to emission peak) within this dip is AT splitting, owing to the dressing effect of $\boldsymbol{E}_1$ ($|G_1|^2/d_{11}$ in $\rho_{44}^{(4)}$) [22].

Now, we turn to the vertical case in Fig. 2(b) and (d). When Δ_1 is set from negative to positive, the EIT separation of PTS [Fig. 2(b1)], suppression separation of FWM signal [Fig. 2(b2)] and the suppression dip as well as emission peak of fluorescence signal [Fig. 2(b3)] move leftwards from bottom to top. However, by setting Δ_2 in similar manner, above mentioned effects disappear [Fig. 2(d)], which demonstrates the difference between the two dressed influences of changing Δ_1 and Δ_2. These phenomena can be explained by the dressed pictures as shown in Fig. 2(e) and (f). With fixed Δ_2 and changing Δ_1, the states $|\pm\rangle$ are fixed. When $\boldsymbol{E}_1$ and $\boldsymbol{E}_4$ match the two-photon condition $\Delta_1 + \Delta_4 = 0$, EIT separation of PTS, suppression separation of FWM and suppression dip of fluorescence will appear. Thus, they move from positive to negative with Δ_1 changing from negative to positive shown as in Fig. 2(b), and this is the two-photon dressed rule reported previously.

However, with fixed Δ_1 and changing Δ_2, the positions of the obtained signals keep invariant with the states $|\pm\rangle$ moving, which means that the signals are fixed with Δ_2 changed, rather than move based on the two-photon condition for the two coupling fields ($\boldsymbol{E}_2$ and $\boldsymbol{E}_4$), i.e., $\Delta_2 + \Delta_4 = 0$ or $\Delta_2 - \Delta_4 = 0$. This phenomenon, as shown in Fig. 2(d), is different from that in Fig. 2(b), and so there maybe exist a new two-photon dressed rule, with which $\boldsymbol{E}_2$ and $\boldsymbol{E}_4$ will comply. It is worth mentioning that the moving states $|\pm\rangle$ will cause the switch between enhancement and suppression of FWM signal (even though this is not observed here). Moreover, the $\boldsymbol{E}_{F2}$ cannot resonate with $|\pm\rangle$ when Δ_4 is scanned at $\Delta_1 = 0$, that is why we can only see the suppression.

From another perspective, the comparison between these two two-photon dressed rules can be explained by density-matrix elements. The EIT separation and suppression separation are produced, which are resulted from the combined dressing effect of $\boldsymbol{E}_1$ and $\boldsymbol{E}_4$, and satisfy $\Delta_4 = (|G_1|^2 - 3\Delta_1^2) \pm (|G_1|^4 - 6|G_1|^2\Delta_1^2 - 3\Delta_1^4)^{1/2}/(2\Delta_1)$, from which one can see that the obtained signals are moved with Δ_1 rather than Δ_2. Similarly, the conditions for AT splitting in fluorescence signals can be obtained as $\Delta_4 = [-\Delta_1 \pm (\Delta_1^2 + 4|G_1|^2)^{1/2}]/2$, which also only

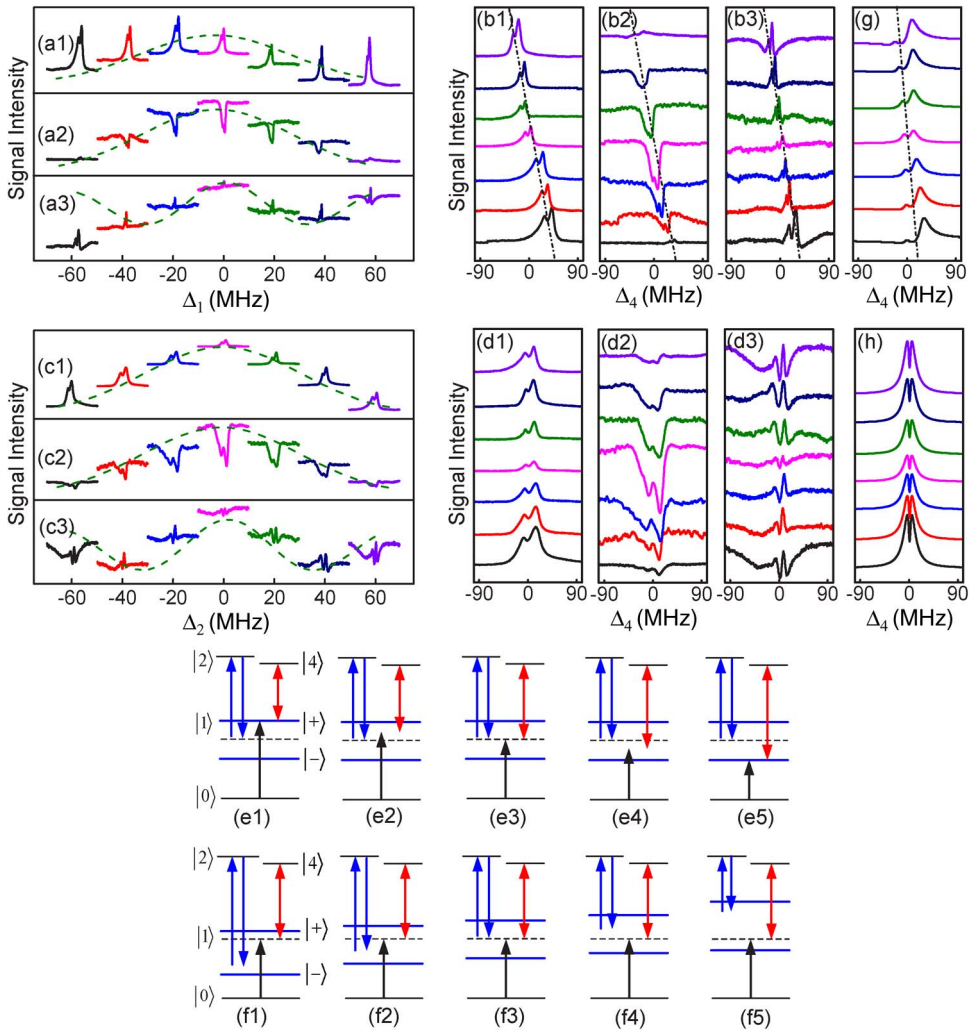

Fig. 2. Measured PTS [(a1) and (b1)], FWM [(a2) and (b2)], and fluorescence signals [(a3) and (b3)] versus Δ_4 at different $\Delta_1 = -60 \sim 60$ MHz [(a) from left to right and (b) from bottom to top] with fixed $\Delta_2 = 0$ and $\boldsymbol{E}_3$ & $\boldsymbol{E}'_3$ & $\boldsymbol{E}'_4$ blocked. (e) Dressed-state pictures corresponding to (a) and (b). (c), (d), and (f) Figure setup is as (a), (b), and (e), but at different $\Delta_2 = -60 \sim 60$ MHz with fixed $\Delta_1 = 0$. Other parameters are $P_1 = 3.8$ mW, $P_2 = 15.9$ mW, $P'_2 = 10.0$ mW, and $P_4 = 46.0$ mW. (g) and (h) Calculated PTS corresponding to (b1) and (d1), respectively.

connects with Δ_1. The interval between the AT splitting peaks is determined by $(\Delta_1^2 + 4|G_1|^2)^{1/2}$, which diminishes from large $|\Delta_1|$ to 0 [Fig. 2(b3)], while remains the same with different Δ_2. The calculated PTS signals are shown in Fig. 2(g) and (h), which agree well with the experimental results in Fig. 2(b1) and (d1), respectively.

If all the beams without $\boldsymbol{E}'_2$ & $\boldsymbol{E}'_4$ are turned on, we can investigate the SWM process (i.e., $\boldsymbol{E}_{S2}$ and $\boldsymbol{E}_{S4}$). The arrangement of the signals is similar with that shown in Fig. 2. The horizontal cases [Fig. 3(a) and (c)] show some similarities and discrepancies with the cases in Fig. 2(a) and (c). On one hand, the upper curves [Fig. 3(a1) and (c1)] show the PTS at discrete values of Δ_1 and Δ_2, which includes EIT separation and an EIT window. The strength of EIT separation is also weak near $\Delta_1 = 0$. The lower curves in Fig. 3(a3) and (c3) show the profiles (dashed lines) that reflect the background intensity of $R_1 + R_2$. On the other hand, the middle curves [Fig. 3(a2) and (c2)] show the SWM signals with AT splitting (dashed line) which is induced by $\boldsymbol{E}_2$. The peak higher than the baseline includes the enhancement of $\boldsymbol{E}_{S2}$ from $\boldsymbol{E}_4$ and double-dressed ($\boldsymbol{E}_2$ & $\boldsymbol{E}_4$ dressed) $\boldsymbol{E}_{S4}$. While the dip lower than the baseline is only the suppression of $\boldsymbol{E}_{S2}$ from $\boldsymbol{E}_4$. For the fluorescence

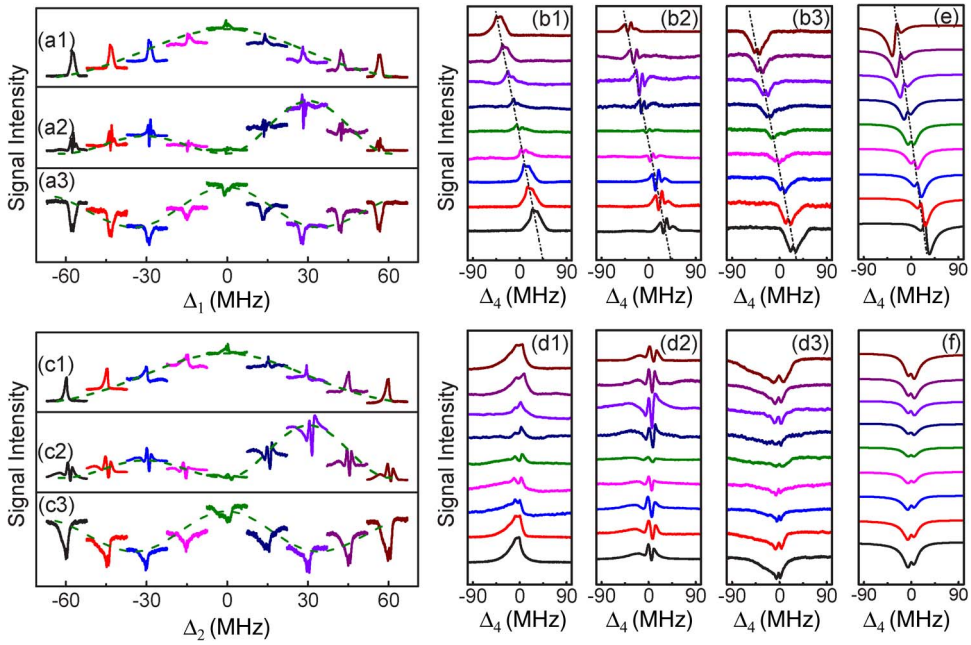

Fig. 3. Figure setup is as Fig. 2 but with $\boldsymbol{E}_2'$ & $\boldsymbol{E}_4'$ blocked. (a2), (b2), (c2), and (d2) are SWM signals. Other parameters are $P_1 = 3.8$ mW, $P_2 = 15.9$ mW, $P_3 = 7.9$ mW, $P_3' = 7.7$ mW, and $P_4 = 46.0$ mW. (e) and (f) Calculated fluorescence signals correspond to (b3) and (d3), respectively.

signal as shown in Fig. 3(b) and (d), one peak within the suppression dip is an emission peak, because of the dressing effect of $\boldsymbol{E}_1$ upon signal R_4.

By setting Δ_1 from negative to positive, the EIT separation of PTS, the enhancement/suppression of SWM signal and suppression dip of fluorescence signal move leftwards from bottom to top as shown in Fig. 3(b). However, they do not move with Δ_2 as shown in Fig. 3(d). The explanation for these phenomena is similar to that for Fig. 2(b) and (d). Here, we only concentrate on the enhancement/suppression of SWM signals. First, from the aspect of the dressed states, with fixed Δ_2 and changing Δ_1, the suppression of SWM also needs to satisfy $\Delta_1 + \Delta_4 = 0$, which results in the movement of the signals in Fig. 3(b); while for the case with fixed Δ_1 and changing Δ_2, the obtained signals are fixed at the same position, which also demonstrates the new two-photon dressed rule for $\boldsymbol{E}_2$ and $\boldsymbol{E}_4$. As to the density-matrix elements, the dressing effects of $\boldsymbol{E}_2$ upon signal $\boldsymbol{E}_{S4}$ and of $\boldsymbol{E}_4$ upon signal $\boldsymbol{E}_{S2}$ are able to be separately written as $|G_2|^2/d_2$ in $\rho_{10S4}^{(5)}$ and $|G_4|^2/d_6$ in $\rho_{10S2}^{(5)}$, from which one can, respectively obtain the suppression and enhancement conditions as $\Delta_1 + \Delta_4 = 0$ and $\Delta_1 + \Delta_4' + [-\Delta_4'/2 \pm (|\Delta_4'|^2 + 4|G_4|^2)^{1/2}/2] = 0$, where $\Delta_4' = \Delta_4 - [\Delta_2 \pm (|\Delta_2|^2 + 4|G_2|^2)^{1/2}]/2$. Therefore, the enhancement and suppression of SWM move leftwards with increased Δ_1, while do not move with Δ_2. The calculated fluorescence signals are depicted by Fig. 3(e) and (f), which agree well with the experimental ones in Fig. 3(b3) and (d3), respectively.

Finally, we present the FWM [Fig. 4(a) and (b)] and SWM processes [Fig. 4(c) and (d)] versus Δ_4 with different Δ_2 when $\boldsymbol{E}_4$ deviates an angle α from the normal state, as shown in Fig. 4(e). The figure setups of Fig. 4(a) and (b) are as Fig. 2(c) and (d). However, in Fig. 4(a1) and (b1), the EIT separation of PTS switches into EIA separation, which indicates that the suppression induced by the combined dressing effects of $\boldsymbol{E}_1$ and $\boldsymbol{E}_4$ (presented by $|G_4|^2/d_6$ in $\rho_{10}^{(1)}$) switches to enhancement. As reported in Ref. [23], in abnormal state, an additional phase factor is introduced and the modulated dressing effect can be presented by $|G_4|^2 exp(i\Delta\phi)/d_6$. Thus, for $\Delta\phi = 0 (\alpha = 0^\circ)$, the dressing term $|G_4|^2 exp(i\Delta\phi)/d_6$ behaves positive and normal EIT separation appears (similar to Fig. 2(c1) and (d1); for $\Delta\phi = -\pi (\alpha = 0.08^\circ)$, the dressing term

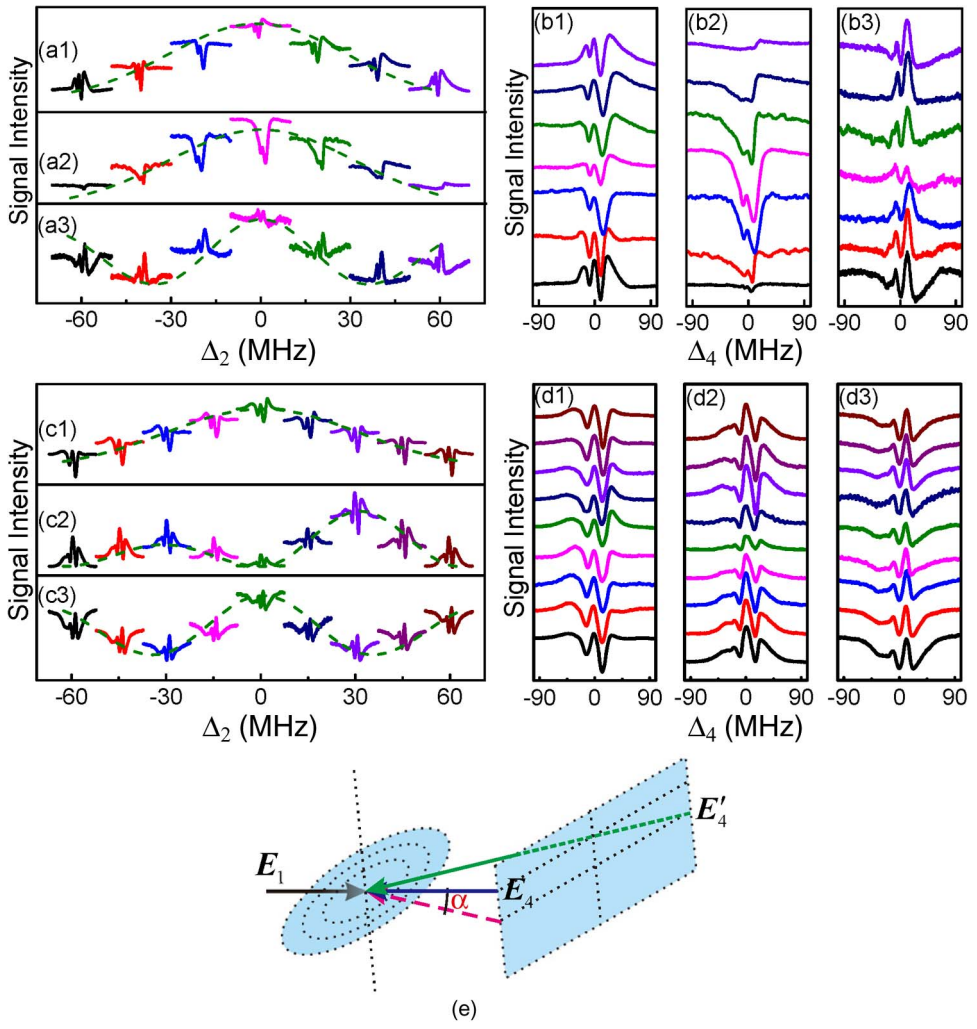

Fig. 4. (a) and (b) Figure setup is as Fig. 2(c) and (d) with $\boldsymbol{E}_3$ & $\boldsymbol{E}'_3$ & $\boldsymbol{E}'_4$ blocked. (c) and (d) Figure setup is as Fig. 3(c) and (d) with $\boldsymbol{E}'_2$ & $\boldsymbol{E}'_4$ blocked. Other parameters are $P_1 = 3.8$ mW, $P_2 = 15.9$ mW, $P'_2 = 10.0$ mW, $P_3 = 7.9$ mW, $P'_3 = 7.7$ mW, and $P_4 = 46$ mW. (e) Spatial configuration of $\boldsymbol{E}_1$ and $\boldsymbol{E}_4$ under abnormal state (solid line) deviating from normal state (dashed line) with a small angle $\alpha = 0.06°$.

$|G_4|^2 exp(i\Delta\phi)/d_6$ behaves negative, so the EIT separation switches to EIA separation; for $\Delta\phi = -\pi/2(\alpha = 0.04°)$, the transitional partial EIT/EIA could be seen. While for the PTS spectra, they behave mainly EIA (EIT) separation if α is larger (smaller) than 0.04°. For the FWM signal as displayed in Fig. 4(a2) and (b2), although it exhibits the suppression separation as before, the intensity of the suppression is weaker than that in Fig. 2(c2) and (d2). Similarly, the suppression dip of fluorescence signals in Fig. 4(a3) and (b3) is shallower than that in Fig. 2(c3) and (d3). All above variations are resulted from that the dressing effect of $\boldsymbol{E}_4$ switches from suppression to enhancement under the influence of particular angle $\alpha = 0.06°(\Delta\phi = -3\pi/4)$.

As to the SWM process, Fig. 4(c) and (d) present the similar profiles and fixed phenomena of measured signals when compared with Fig. 3(c) and (d), respectively. However, the EIT separation of PTS in Fig. 4(d1) also switches into EIA separation, owing to the modulated dressing effects $|G_4|^2 exp(i\Delta\phi)/d_6$ at $\alpha = 0.06°$ (greater than 0.04°). The intensity of the peak of SWM signal in Fig. 4(c2) and (d2) is stronger than that in Fig. 3(c2) and (d2). At the same time, the AT splitting emission peaks of the fluorescence signal in Fig. 4(c3) and (d3) are higher than those in Fig. 3(c3) and (d3). Above phenomena also demonstrate that the dressing effect of $\boldsymbol{E}_4$ will switch from suppression to enhancement at this particular angle.

4. Conclusion

In summary, we have compared the traditional and novel two-photon dressed rules by changing Δ_1 and Δ_2, separately. We have demonstrated that the EIT of PTS, the enhancement/suppression of MWM, and the accompany fluorescence signals with AT splitting move with Δ_1 but do not move with Δ_2, which illustrates the essence of traditional and novel dressed rules, respectively. In addition, we have revealed that the dressed strength of $\boldsymbol{E}_4$ is determined by the minimum interval between the probe field $\boldsymbol{E}_1$ and dressed state induced by the coupling field $\boldsymbol{E}_2$. Finally, we have studied the switches of PTS, MWM, and fluorescence signals at another angle between $\boldsymbol{E}_1$ and $\boldsymbol{E}_4$ to demonstrate the phase control effects. The research has potential applications in signal processing, optical switch prototype fabrications, and quantum communications.

References

[1] Y. P. Zhang, A. W. Brown, and M. Xiao, "Opening four-wave mixing and six-wave mixing channels via dual electromagnetically induced transparency windows," *Phys. Rev. Lett.*, vol. 99, no. 12, pp. 123603-1–123603-4, Sep. 2007.

[2] Z. C. Zuo, J. Sun, X. Liu, Q. Jiang, G. S. Fu, L. A. Wu, and P. M. Fu, "Generalized n-photon resonant 2n-wave mixing in an (n + 1)-level system with phase-conjugate geometry," *Phys. Rev. Lett.*, vol. 97, no. 19, pp. 193904-1–193904-4, Nov. 2006.

[3] S. E. Harris, "Electromagnetically induced transparency," *Phys. Today*, vol. 50, no. 7, pp. 36–42, Jul. 1997.

[4] K. J. Boller, A. Imamolu, and S. E. Harris, "Observation of electromagnetically induced transparency," *Phys. Rev. Lett.*, vol. 66, no. 20, pp. 2593–2596, May 1991.

[5] M. D. Lukin and A. Imamolu, "Controlling photons using electromagnetically induced transparency," *Nature*, vol. 413, no. 6853, pp. 273–276, Sep. 2001.

[6] C. Liu, Z. Dutton, C. H. Behroozi, and L. V. Hau, "Observation of coherent optical information storage in an atomic medium using halted light pulses," *Nature*, vol. 409, no. 6819, pp. 490–493, Jan. 2001.

[7] L.-M. Duan, M. D. Lukin, J. I. Cirac, and P. Zoller, "Long-distance quantum communication with atomic ensembles and linear optics," *Nature*, vol. 414, no. 6862, pp. 413–418, Nov. 2001.

[8] M. D. Lukin, A. B. Matsko, M. Fleischhauer, and M. O. Scully, "Quantum noise and correlations in resonantly enhanced wave mixing based on atomic coherence," *Phys. Rev. Lett.*, vol. 82, no. 9, pp. 1847–1850, Mar. 1999.

[9] Y. Li and M. Xiao, "Enhancement of nondegenerate four-wave mixing based on electromagnetically induced transparency in rubidium atoms," *Opt. Lett.*, vol. 21, no. 14, pp. 1064–1066, Jul. 1996.

[10] Y. P. Zhang, A. W. Brown, and M. Xiao, "Observation of interference between four-wave mixing and six-wave mixing," *Opt. Lett.*, vol. 32, no. 9, pp. 1120–1122, May 2007.

[11] Y. P. Zhang and M. Xiao, "Enhancement of six-wave mixing by atomic coherence in a four-level inverted Y system," *Appl. Phys. Lett.*, vol. 90, no. 11, pp. 111104-1–111104-3, Mar. 2007.

[12] C. Chen, Y. Y. Yin, and D. S. Elliott, "Interference between optical transitions," *Phys. Rev. Lett.*, vol. 64, no. 5, pp. 507–510, Jan. 1990.

[13] R. Yamazaki and D. S. Elliott, "Observation of the phase lag in the asymmetric photoelectron angular distributions of atomic barium," *Phys. Rev. Lett.*, vol. 98, no. 5, pp. 053001-1–053001-4, Jan. 2007.

[14] S. H. Autler and C. H. Townes, "Stark effect in rapidly varying fields," *Phys. Rev.*, vol. 100, no. 2, pp. 703–722, Oct. 1955.

[15] J. B. Qi, G. Lazarov, X. J. Wang, L. Li, L. M. Narducci, A. M. Lyyra, and F. C. Spano, "Autler-Townes splitting in molecular lithium: Prospects for all-optical alignment of nonpolar molecules," *Phys. Rev. Lett.*, vol. 83, no. 2, pp. 288–291, Jul. 1999.

[16] O. D. Mücke, T. Tritschler, M. Wegener, U. Morgner, and F. X. Kärtner, "Role of the carrier-envelope offset phase of few-cycle pulses in nonperturbative resonant nonlinear optics," *Phys. Rev. Lett.*, vol. 89, no. 12, pp. 127401-1–127401-4, Aug. 2002.

[17] Y. P. Zhang, Z. Q. Nie, Z. G. Wang, C. B. Li, F. Wen, and M. Xiao, "Evidence of Autler-Townes splitting in high-order nonlinear processes," *Opt. Lett.*, vol. 35, no. 20, pp. 3420–3422, Oct. 2010.

[18] Y. P. Zhang, P. Y. Li, H. B. Zheng, Z. G. Wang, H. X. Chen, C. B. Li, R. Y. Zhang, and M. Xiao, "Observation of Autler-Townes splitting in six-wave mixing," *Opt. Exp.*, vol. 19, no. 8, pp. 7769–7777, Apr. 2011.

[19] J. Qi, F. C. Spano, T. Kirova, A. Lazoudis, J. Magnes, L. Li, L. M. Narducci, R. W. Field, and A. M. Lyyra, "Measurement of transition dipole moments in lithium dimers using electromagnetically induced transparency," *Phys. Rev. Lett.*, vol. 88, no. 17, pp. 173003-1–173003-4, Apr. 2002.

[20] J. Qi and A. M. Lyyra, "Electromagnetically induced transparency and dark fluorescence in a cascade three-level diatomic lithium system," *Phys. Rev. A, At. Mol. Opt. Phys.*, vol. 73, no. 4, pp. 043810-1–043810-9, Apr. 2006.

[21] N. Li, Z. Y. Zhao, H. X. Chen, P. Y. Li, Y. H. Li, Y. Zhao, G. Z. Zhou, S. Q. Jia, and Y. P. Zhang, "Observation of dressed odd-order multi-wave mixing in five-level atomic medium," *Opt. Exp.*, vol. 20, no. 3, pp. 1912–1929, Jan. 2012.

[22] G. Huang, Y. Zhang, Z. Zhang, X. Yao, J. Che, H. Zheng, and Y. Zhang, "Evidence of Autler-Townes splitting in fluorescence and six-wave mixing with multi-electromagnetically induced transparency," *J. Opt. Soc. Amer. B, Opt. Phys.*, vol. 30, no. 9, pp. 2563–2569, Sep. 2013.

[23] P. Y. Li, Z. Y. Zhao, Z. G. Wang, Y. Q. Zhang, H. Y. Lan, H. X. Chen, H. B. Zheng, and Y. P. Zhang, "Phase control of bright and dark states in four-wave mixing and fluorescence channels," *Appl. Phys. Lett.*, vol. 101, no. 8, pp. 081107-1–081107-4, Aug. 2012.